ChemCatChem

Research Article
doi.org/10.1002/cctc.202400777

Chemistry Europe
European Chemical Societies Publishing

www.chemcatchem.org

Avoiding Replicates in Biocatalysis Experiments: Machine Learning for Enzyme Cascade Optimization

Regine Siedentop,[a] Maximilian Siska,[b] Johanna Hermes,[a] Stephan Lütz,[a] Eric von Lieres,*[b, c] and Katrin Rosenthal*[d]

The optimization of enzyme cascades is a complex and resource-demanding task due to the multitude of parameters and synergistic effects involved. Machine learning can support the identification of optimal reaction conditions, for example, in the case of Bayesian optimization (BO), by proposing new experiments based on Gaussian process regression (GPR) and expected improvement (EI). Here, in this research BO is used to optimize the concentrations of the reaction components of an enzyme cascade. The productivity-cost-ratio is chosen as the optimization objective in order to achieve the highest possible productivity, which was normalized to the costs of the materials used to prevent convergence to ever-increasing enzyme concentrations. To reduce the experimental effort, contrary to common practice in biological experiments, replicates were not used; instead, the algorithm's proposed experiments and inherent uncertainty quantification were relied upon. This approach balances parameter space exploration and exploitation, which is critical for the efficient and effective identification of optimal reaction conditions. At the optimized reaction conditions identified in this study, the productivity-cost ratio is doubled to 38.6 mmol L^{-1} h^{-1} €$^{-1}$ compared to a reference experiment. The parameter optimization required only 52 experiments while being robust to outlying experimental results.

1. Introduction

Biocatalysis is playing an increasingly important role in the synthesis of complex molecules, which is further driven by the availability of new enzymes and their targeted development.[1–4] The combination of two or more enzymes in one pot, called an enzyme cascade, expands the possibilities for the synthesis of complex molecules.[5–8] The development of these in vitro enzyme cascades poses the challenge of a continuous cofactor regeneration, of the energy supply in the form of adenosine-5′-triphosphate (ATP).[9,10] Therefore, several enzymatic ATP regenerating systems were established, such as polyphosphate kinases, acetate kinase (ACK), or pyruvate kinase.[11–14] ATP regeneration by ACK uses acetyl phosphate as phosphate donor, which can be synthesized in situ by oxidation and decarboxylation of pyruvate and phosphate by pyruvate oxidase (POX).[15–17] Hence, the stability and economic drawbacks of acetyl phosphate as phosphate donor are bypassed.[18] Furthermore, the redox reaction of POX can be coupled to electrochemical methods.[18,19] Beyond continuous cofactor regeneration, the performance of in vitro enzyme cascades is influenced by many parameters, including the composition and concentration of reaction components, pH, and temperature. For a large-scale application, the ecology of the reaction also plays a pivotal role.[2] Identifying the optimal reaction conditions is a complex task and utilizing computational methods can streamline the optimization process.[20,21]

Bayesian optimization (BO), also referred to as active learning in the context of process optimization, is a class of machine-learning algorithms that can be particularly useful for such multi-dimensional and multi-objective optimization problems.[22–26] BO is suitable for black-box systems, in which a detailed and mechanistic understanding of the reaction network is not required.[27] Effects such as inhibitions or side-reactions have thus not to be known for a comprehensive optimization. It involves a surrogate model such as Gaussian process regression (GPR) combined with an acquisition function such as expected improvement (EI). In this context, GPR predicts the relation between parameter values such as concentrations or pH and key performance indicators (KPI) such as yield or productivity. Most importantly, it also predicts the uncertainty of these KPIs.[27,28] The GPR model is sequentially refined as more experimental data become available. In each successive round, new measurement points are

[a] R. Siedentop, J. Hermes, S. Lütz
Department of Biochemical and Chemical Engineering, TU Dortmund University, Emil-Figge-Straße 66, 44227 Dortmund, Germany

[b] M. Siska, E. von Lieres
Institute of Bio- and Geosciences, Forschungszentrum Jülich GmbH, Wilhelm-Johnen-Straße, 52428 Jülich, Germany
E-mail: e.von.lieres@fz-juelich.de

[c] E. von Lieres
Computational Systems Biotechnology, RWTH Aachen University, Forckenbeckstraße 51, 52074 Aachen, Germany

[d] K. Rosenthal
School of Science, Constructor University, Campus Ring 6, 28759 Bremen, Germany
E-mail: krosenthal@constructor.university

Regine Siedentop and Maximilian Siska contributed equally to this work.

Supporting information for this article is available on the WWW under https://doi.org/10.1002/cctc.202400777

proposed, guided by the prediction of the highest EI of a KPI, as determined by the GPR model. The acquisition function quantifies a trade-off between parameter regions with expected optimal values (exploitation) and regions with high uncertainty of the GPR prediction due to sparse data coverage (exploration).[29] During BO, synergistic effects between all components of the whole system are simultaneously responded to by concurrently adjusting all parameters and not only one factor at a time.[30] Nonetheless, the optimum is identified with a defined parameter set for the given objective and within a predefined window of operation. BO is already used in many disciplines and has attracted increasing attention in the biocatalytic field in recent years.[27,31–37]

In this study, we used the ATP regeneration system consisting of ACK and POX for the phosphorylation of mevalonate (MVA) to mevalonate phosphate (MVAP) catalyzed by mevalonate kinase (MVK), which are important intermediates in the isoprenoid pathway for the synthesis of terpenes.[38–41] In in vitro approaches, ATP regeneration has been shown to be a critical factor in the performance of product synthesis, as indicated in mechanistic modeling studies.[41–44] In a previous study, we successfully coupled the ATP regeneration to electrochemistry; however, a more holistic optimization of the compound concentrations would be beneficial for higher yields and cofactor utilization.[18] Here, we use productivity of the MVK-catalyzed reaction as optimization objective for the process optimization and a combined optimization of productivity and costs introduced as productivity-cost ratio (Pr/€). This approach was chosen in order to increase productivity while at the same time taking costs into account and avoiding convergence towards ever higher enzyme concentrations. In addition, we monitored other KPIs, that is, conversion, space-time-yield (STY), enzyme activity, and cost of the reaction components.

The optimization process utilized GPR as a surrogate model and EI as the acquisition function. This strategic approach involves proposing sampling locations that carefully balance the exploration of under-investigated regions within the parameter space, characterized by low sampling density, and exploiting the most promising areas by proposing additional experiments close to the best-performing measurements. Since biological experiments can be complicated, replicate measurements are often performed to ensure experiment performance, significance, and reproducibility. In contrast to this common practice in biocatalytic experimentation, we decided against replicating individual measurements. This decision was made in favor of increasing the number of unique measurements and therefore maximizing the information derived from the experiments. By doing so, we aim to enhance our understanding of the intricate functional relationship between the studied parameters, which is critical to efficiently and effectively identifying the region of optimality.

While traditional point-wise methods do require replicates to assess the uncertainty of the final optimal value, the applied Gaussian process inherently estimates not only the mean value but also the standard deviation of the approximated functional relationship at any point of the design space. This estimation is based not only on a single measurement but considers experimental data in a neighborhood of the optimal point. In the exploration phase of the BO algorithm, many points are distributed closely around the optimal point rather than repeating a single measurement. Hence, this method effectively allows to avoid replicates also in the presence of technical errors. Kreyling et al. have also found that it is generally more informative to distribute a given number of measurements in a region around the optimum rather than perform replicates at fewer points.[45] Experimental replicates can be useful for calibrating mechanistic error models.[46] However, such error models are not trivial to establish for the studied non-linear processes and are out of the scope of publication.

Table 1. Parameter space with studied parameters and their ranges. ACK: acetate kinase; ADP: adenosine-5′-diphosphate; MVA: mevalonate; MVK: mevalonate kinase; POX: pyruvate oxidase.

Compound	Concentration Parameter Range
MVA	10–30 mM
ADP	1–30 mM
Phosphate	10–200 mM
Pyruvate	Respective to c(MVA) + 5 mM
POX	0.1–10 U mL^{-1}
ACK	0.1–10 U mL^{-1}
MVK	10–200 mg L^{-1}

2. Results and Discussion

2.1. ATP Regeneration by Pyruvate Oxidase and Acetate Kinase

For the optimization process, enzyme, and substrate concentrations (MVA, ADP, phosphate, pyruvate, POX, ACK, and MVK concentrations) were chosen as adjustable parameters to achieve the maximum performance of the enzyme cascade (Figure 1). Temperature and pH were not included as parameters to keep the design space narrow and the complexity low. Concentrations were chosen to define the parameter space in which the optimum is expected and sought.

As substrate for the main product MVAP, MVA is added with initial concentration ranges between 10 to 30 mM (Table 1). MVA is an expensive substrate, that is why the concentration range was kept narrow. In later experiments (Bayesian optimization), the concentration of MVA was kept constant and was excluded for the calculation of the productivity-cost ratio, as it would have dominated the cost-factor (>98%). Pyruvate is added in slight excess to MVA, while ADP is added in concentrations of 1 mM for mandatory ADP regeneration up to the stoichiometric amount of MVA. Phosphate has a wider range of 10 to 200 mM because on the one hand, it may exhibit inhibitory properties; on the other hand, at higher concentrations, it has the potential to shift the reaction equilibrium favorably towards the product side. According to previous knowledge available for MVK, an upper limit of 200 mg L^{-1} was chosen.[18,47] For ACK, the homologues from *Acholeplasma laidlawii* (*Al*ACK), *Clostridium acetobutylicum* (*Ca*AcK), *Shewanella* (SACK), *Escherichia coli* (*Ec*ACK) were tested.

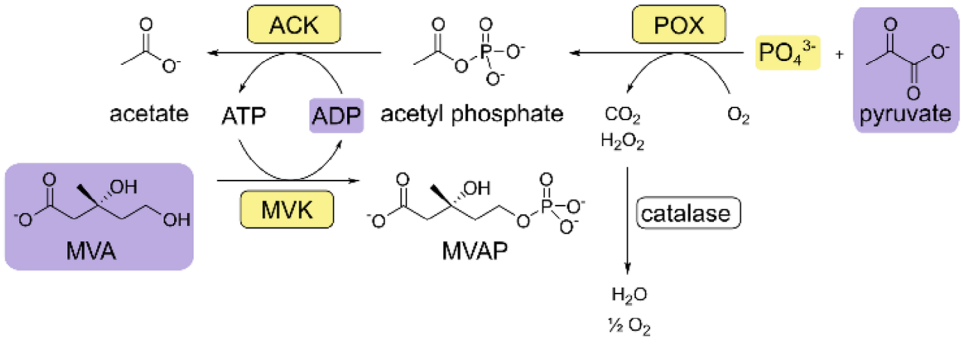

Figure 1. ATP regeneration by pyruvate oxidase and acetate kinase for the phosphorylation of mevalonate by mevalonate kinase. The concentrations of marked compounds were varied to optimize productivity and productivity-cost ratio of the enzyme cascade. Yellow-marked compounds were the focus of the proceeded optimization process. ACK: acetate kinase, MVA: mevalonate, MVAP: mevalonate phosphate, MVK: mevalonate kinase, POX: pyruvate oxidase.

SACK could not be successfully expressed. The other three ACKs showed similar reaction rates in the enzyme cascade (Figure S2). As slightly higher product concentrations could be detected with the *Ca*ACK after 24 h, this enzyme was selected for the further experiments. For reasons of clarity, the enzyme is abbreviated as ACK in the following. For POX, it turned out that POX is difficult to express and results in low expression levels.[48] Therefore, a commercially available enzyme of *Aerococcus viridans* was used. Hence, POX was the cost-driving factor compared to the overall costs of the enzyme cascade (Table S3). For both enzymes, a more comprehensive range of 0.1 to 10 U mL^{-1} was chosen as less experience exists for these enzymes.

2.2. Initial Screening of the Parameter Space

The seven selected parameters create a high-dimensional parameter space in which the optimal composition of the enzyme cascade needs to be found. To assess the individual impact of each parameter on productivity, we initially employed a one-factor-at-a-time (OFAT) approach, conducting experiments at the boundary values for each parameter. Logarithmically centered parameter values were selected as basis for the OFAT experiments, which aligns with the log-transformation of GPR input data as outlined in the section on GPR modeling. A reference experiment was also performed using the experimental conditions of the logarithmically centered parameter values.

In addition, based on the initial OFAT experiments, an additional round of experiments with increased concentrations of pyruvate, phosphate, or POX, and with varied concentrations of ADP were performed to validate the bounds of the parameter space. The experimental conditions and results of the two-rounds of OFAT experiments are shown in Table 2. As mentioned before, all experiments were conducted without replicates. In addition to productivity, conversion, STY, enzyme activity, and costs (Table S3) of the reaction components were calculated.

Increased concentrations of enzymes led to increased productivities (Experiments A1.8, A1.10, A1.12, and A2.8) and especially the increased concentration of POX to 20 U mL^{-1} resulted in the highest productivity of 60.2 mmol L^{-1} h^{-1} (Experiment A2.8). Elevated concentrations of pyruvate positively affect productivity, while ADP has less influence (Experiments A2.2 and A1.3, A1.4, A2.6, A2.7). Varying concentrations of MVA have only marginal influence on productivity and since it is an expensive substrate, it was excluded from further variations.

Other KPIs such as conversion, STY or activity have shown other trends compared to the productivity. The conversion was above 80% in all initial experiments, except when using 0.1 U mL^{-1} POX (Experiment A1.7). Using this condition, all KPIs except for the productivity-cost ratio are the lowest. Using higher amounts of POX has a positive influence on activity and productivity but increases the costs, which in turn lowers the productivity-cost ratio (Experiments A1.8 and A2.8). The productivity-cost ratio was enhanced using increased amounts of ACK, phosphate, pyruvate, while maintaining medium amounts of ADP (Experiments A1.6, A1.9, A1.10, A2.2, A2.6, and A2.7). The STY varied between 1.6 g L^{-1} d^{-1} and 5.1 g L^{-1} d^{-1} (Experiments A1.7 and A2.2), and activity remained between 0.5 U mg^{-1} and 15.0 U mg^{-1} (Experiments A1.7 and A1.11). The most promising conditions resulting in the highest productivity values were combined in a third-round of experiments to gain further information about the reaction (Table 3).

Overall, the combination of the conditions resulted in increased productivities. Especially high concentrations of phosphate, POX and ACK led to the highest productivity with 77.2 mmol L^{-1} h^{-1} (Experiment A3.3). However, increased amounts of POX escalate the costs of the process and ultimately lower the productivity-cost ratio. Conversions remained between 83% and 88% (Experiments A3.4 and A3.6) and STY and activity also remained in a similar range as the previous experiments with 2.6 g L^{-1} d^{-1} to 3.9 g L^{-1} d^{-1} (Experiments A3.6 and A3.5) and 2.7 U mg^{-1} to 14.5 U mg^{-1} (Experiments A3.2, A3.3, and A3.4), respectively. Still, higher productivities are expected and the results were used to narrow the parameter space and to initialize BO for identifying the optimal conditions.

To narrow the parameter space for further optimization, the impact of each design parameter was analyzed. For this purpose, productivity was plotted as a function of concentration parameters (Figure 2). POX has the highest influence on productivity, while phosphate and MVK show a reduced impact at the upper concentration range. Varying MVA and ADP concentrations change the productivity marginally in the chosen concentration ranges. Therefore, the parameter space was adapted to these findings by keeping MVA and ADP concen-

Table 2. Results of the two-rounds of OFAT experiments. If not mentioned otherwise, concentrations were 44.7 mM PO_4^{3-}, c(MVA)+5 mM pyruvate, 5.5 mM ADP, 17.3 mM MVA, 80 mg L^{-1} MVK, 1 U mL^{-1} ACK und 1 U mL^{-1} POX in Tris-based buffer (100 mM Tris-HCl, 150 mM NaCl, 10% glycerol, 20 mM of $MgCl_2$, pH 7.5; with additionally added 0.1 mM FAD, 0.1 mM ThPP, 20 U mL^{-1} catalase, 3 mM Na_3VO_4, 0.043 mM $NADP^+$, 0.43 mM CoA, 170 mM glucose, 200 mM NaOAc, and 20 mM $MgCl_2$). Assays were performed in singlicates at 30 °C and 30 rpm using a multirotator. MVA was not included in the cost calculation, as it accounts for >98% of the costs. Conversions were determined after 24 h. Results were colored for each round of experiments according to their value (lowest - white, higher - darker). STY: space-time-yield; Pr/€: productivity-cost ratio.

Experiment	Parameter	Concentration	Conversion [%]	STY [g L^{-1} d^{-1}]	Activity [U mg^{-1}]	Productivity [mmol L^{-1} h^{-1}]	Costs [€]	Pr/€ [mmol L^{-1} h^{-1} €$^{-1}$]
reference	–	–	89	2.9	3.2	18.7	0.97	19.2
A1.1	MVA	10 mM	89	1.7	3.6	16.2	0.97	16.6
A1.2	MVA	30 mM	66	4.4	2.3	16.0	0.97	16.4
A1.3	ADP	1 mM	90	3.0	4.0	18.8	0.96	19.5
A1.4	ADP	30 mM	59	3.2	2.3	17.6	1.01	17.3
A1.5	PO_4^{3-}	10 mM	60	2.1	1.9	11.6	0.97	11.9
A1.6	PO_4^{3-}	200 mM	91	3.1	5.0	22.7	0.97	23.4
A1.7	POX	0.1 U mL^{-1}	29	1.6	0.5	4.7	0.31	15.5
A1.8	POX	10 U mL^{-1}	89	2.9	7.7	32.4	7.62	4.3
A1.9	ACK	0.1 U mL^{-1}	89	3.0	3.3	22.6	0.97	23.3
A1.10	ACK	10 U mL^{-1}	86	3.2	3.1	25.1	0.97	25.8
A1.11	MVK	10 mg L^{-1}	90	3.1	15.0	10.0	0.97	10.3
A1.12	MVK	200 mg L^{-1}	88	3.0	1.6	19.6	0.97	20.1
A2.1	Dilution	1:1	84	2.2	3.2	8.8	0.60	14.8
A2.2	Pyruvate	100 mM	88	5.1	3.3	23.6	0.97	24.2
A2.3	PO_4^{3-}	120 mM	88	2.9	4.3	19.7	0.97	20.3
A2.4	PO_4^{3-}	300 mM	89	2.7	4.5	18.6	0.97	19.2
A2.5	PO_4^{3-}	400 mM	89	4.1	3.5	21.2	0.97	21.8
A2.6	ADP	2.5 mM	88	3.5	3.7	23.1	0.97	23.9
A2.7	ADP	11 mM	89	4.0	3.0	23.1	0.98	23.5
A2.8	POX	20 U mL^{-1}	88	3.6	10.1	60.2	15.00	4.0

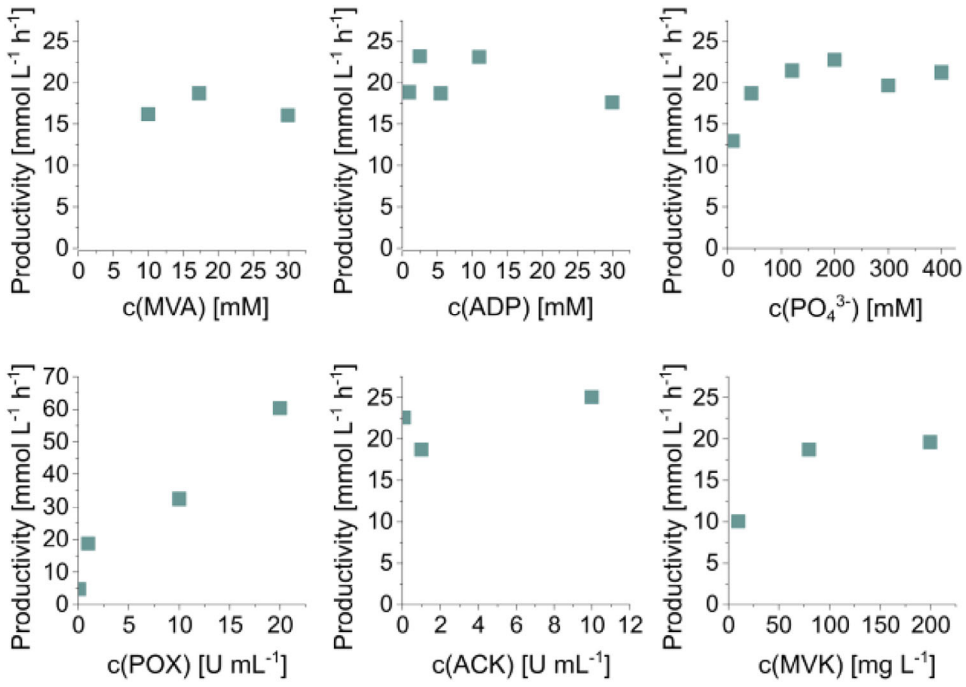

Figure 2. Impact of concentration parameters on productivity.

Table 3. Combinations of promising OFAT conditions. If not mentioned otherwise, concentrations were 44.7 mM PO_4^{3-}, 22.3 mM pyruvate, 5.5 mM ADP, 17.3 mM MVA, 80 mg L^{-1} MVK, 1 U mL^{-1} ACK und 1 U mL^{-1} POX in Tris-based buffer (100 mM Tris-HCl, 150 mM NaCl, 10% glycerol, 20 mM of $MgCl_2$, pH 7.5; with additionally added 0.1 mM FAD, 0.1 mM ThPP, 20 U mL^{-1} catalase, 3 mM Na_3VO_4, 0.043 mM $NADP^+$, 0.43 mM CoA, 170 mM glucose, 200 mM NaOAc, and 20 mM $MgCl_2$). Assays were performed in singlicates at 30 °C and 30 rpm in a multirotator. MVA was not included in the cost calculation, as it accounts for >98% of the costs. Conversions were determined after 24 h. Results were colored for each round of experiments according to their value (lowest - white, higher - darker). STY: space-time-yield; Pr/€: productivity-cost ratio.

Experiment	Concentration	Conversion [%]	STY [g L^{-1} d^{-1}]	Activity [U mg^{-1}]	Productivity [mmol L^{-1} h^{-1}]	Costs [€]	Pr/€ [mmol L^{-1} h^{-1} €$^{-1}$]
reference	–	89	2.9	3.2	18.7	0.97	19.2
A3.1	200 mM PO_4^{3-} 10 U mL^{-1} POX	88	3.8	6.3	45.1	7.62	5.9
A3.2	200 mM PO_4^{3-} 10 U mL^{-1} POX 200 mg L^{-1} MVK	88	3.6	2.7	46.3	7.62	6.1
A3.3	200 mM PO_4^{3-} 10 U mL^{-1} POX 10 U mL^{-1} ACK	88	3.4	14.5	77.2	7.62	10.1
A3.4	200 mg L^{-1} MVK 10 U mL^{-1} POX 10 U mL^{-1} ACK	83	3.7	2.7	37.8	7.62	5.0
A3.5	200 mM PO_4^{3-} 10 U mL^{-1} POX 10 U mL^{-1} ACK 200 mg L^{-1} MVK	85	3.9	2.8	42.3	7.62	5.6
A3.6	200 mM PO_4^{3-} 200 mM pyruvate 10 U mL^{-1} POX 10 U mL^{-1} ACK 200 mg L^{-1} MVK	88	2.6	3.9	44.2	7.62	5.8

Table 4. Adapted parameter space for BO.

Compound	Tested Concentrations
MVA	Constant at 17.3 mM
ADP	Constant at 1.0 mM
PO_4^{3-}	10–200 mM
Pyruvate	Respective to c(PO_4^{3-})
POX	0.1–10 U mL^{-1}
ACK	0.1–10 U mL^{-1}
MVK	10–200 mg L^{-1}

trations constant at 17.3 mM and 1.0 mM, respectively (Table 4). Pyruvate, which showed an influence on the KPIs, is added in stoichiometric amounts to phosphate to expand the concentration range of the former parameter.

With the obtained knowledge, the 4 parameters phosphate, POX, ACK, and MVK constitute the adapted parameter space for the iterative BO. Consequently, every sampling location proposed during the BO represents a distinct combination of these parameters.

2.3. Bayesian Optimization

Using all previously obtained data and the adapted parameter space, four- rounds of BO were performed. In the first two rounds, up to eight experiments were conducted, which was reduced to four in the following rounds, as the suggested sampling locations were relatively similar (Table S2). Performing one experiment per round would be ideal but is impractical due to lab organization and time limitations.[33] In the first BO round, the process was optimized with respect to maximizing productivity. In subsequent rounds, the optimization objective was changed to the productivity-cost ratio, because further increase in productivity would require higher enzyme quantities[34] which are unfavorable from an economic perspective.[44] Other factors such as sustainability could have also been chosen, depending on the necessity and goal of the optimization.[49,50] Experimental conditions and their results are shown in Table 5. Additionally, Figure 3 presents an overview of the results of the initial explorative experiments and of the subsequent BO.

During the first BO round, the observed productivity reaches 25.8 mmol L^{-1} h^{-1}, which is less than measured in the exploratory rounds (Experiment B1.1). Considering that the exploratory rounds consisted of OFAT experiments, an increase in productivity during this round was not anticipated. The first BO round primarily serves an exploratory purpose as the algorithm aims to obtain more information on sparsely sampled areas of the parameter space. In the second BO round, when the objective function was switched to the productivity-cost ratio, this KPI increased to 24.2 mmol L^{-1} h^{-1} €$^{-1}$ (Experiment B2.3) in comparison to the previous BO round. Interestingly, several experiments were proposed with similar conditions to experiment A1.10, which showed the best productivity-cost ratio in the

Table 5. Conditions and results of the four BO rounds. The assays contained the mentioned concentrations of PO_4^{3-}, POX, ACK, and MVK. Other added compounds were 1 mM ADP, 17.3 mM MVA, in Tris-based buffer (100 mM Tris-HCl, 150 mM NaCl, 10% glycerol, 20 mM of $MgCl_2$, pH 7.5; with additionally added 0.1 mM FAD, 0.1 mM ThPP, 20 U mL^{-1} catalase, 3 mM Na_3VO_4, 0.043 mM $NADP^+$, 0.43 mM CoA, 170 mM glucose, 200 mM NaOAc, and 20 mM $MgCl_2$). Assays were performed in singlicates at 30 °C and 30 rpm in a multirotator. MVA was not included in the cost calculation, as it accounts for >98% of the costs. Results were colored for each BO round of experiments according to their value (lowest – white, higher – darker). Pr/€: productivity-cost ratio.

Experiment	Pyruvate and PO_4^{3-} [mM]	POX [U mL^{-1}]	ACK [U mL^{-1}]	MVK [mg L^{-1}]	Productivity [mmol L^{-1} h^{-1}]	Costs [€]	Pr/€ [mmol L^{-1} h^{-1} $€^{-1}$]	Optimization objective
reference	44.7	1.0	1.0	80	18.7	0.97	19.2	–
B1.1	95.6	2.2	4.2	163.9	25.8	1.88	13.7	Productivity
B1.2	49.0	7.8	5.1	12.8	8.8	6.00	1.5	
B1.3	19.0	0.1	1.0	183.4	3.4	0.33	10.3	
B1.4	35.6	2.1	2.2	43.9	15.0	1.77	8.5	
B1.5	14.0	0.5	0.4	24.2	4.8	0.58	8.3	
B1.6	106.3	0.3	3.9	59.7	7.9	0.41	19.1	
B1.7	53.9	1.3	0.5	51.9	10.9	1.19	9.1	
B2.1	48.7	0.6	10	91	14.6	0.70	20.7	Productivity-cost-ratio
B2.2	110.6	0.6	1.3	114.9	15.6	0.65	24.0	
B2.3	200	0.5	0.6	132.4	14.2	0.59	24.2	
B2.4	49.5	0.7	10	86.5	15.4	0.73	21.1	
B2.5	96.1	0.6	0.1	171.7	13.5	0.64	21.0	
B2.6	44.1	0.7	10	87.8	15.9	0.75	21.2	
B2.7	76.5	0.6	1.6	105.2	14.8	0.69	21.5	
B2.8	58	0.7	10	76.9	15.4	0.77	20.0	
B3.1	200	0.5	1	109.8	19.2	0.60	31.9	
B3.2	153.9	0.6	0.8	123.8	19.9	0.64	31.0	
B3.3	200	0.5	0.8	92.4	15.7	0.58	27.1	
B3.4	200	0.6	1	135.3	17.9	0.66	27.2	
B4.1	200	0.4	1	135.8	20.6	0.53	38.6	
B4.2	200	0.4	1	130.3	20.4	0.54	37.4	
B4.3	200	0.4	1	126.7	19.8	0.55	35.9	
B4.4[a]	200	0.4	1	135.8	21.5	0.54	39.8	

[a] 5.5 mM ADP instead of 1 mM.

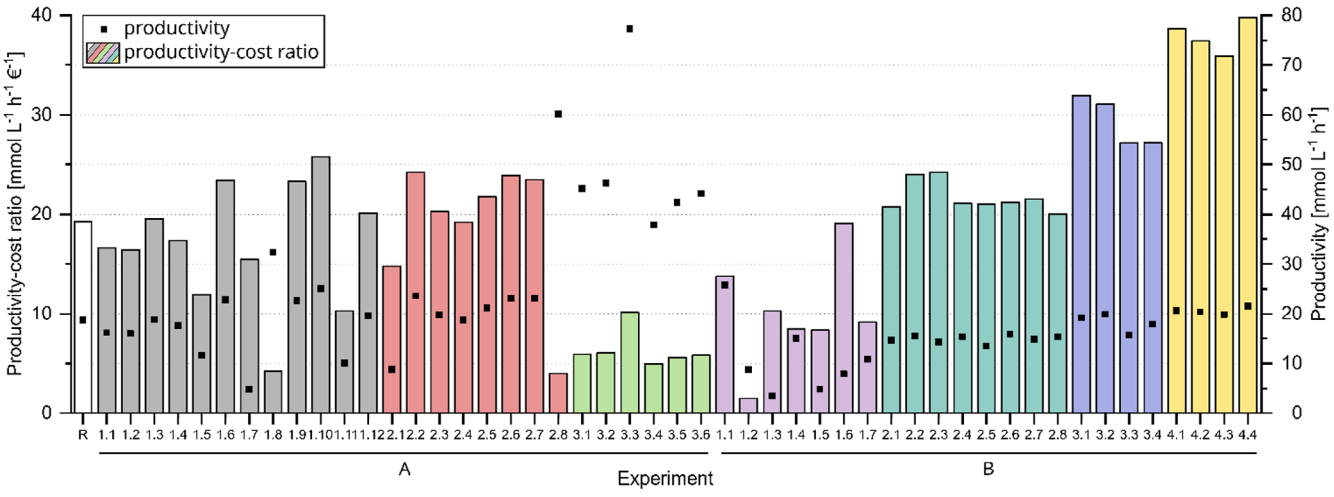

Figure 3. Overview of productivity and productivity-cost ratio of the explorative experiments (A1-A3) and of the subsequent BO (B1-B4). Optimization objectives were productivity (black dots) for experiments A1-B1 and productivity-cost ratio (columns) for experiments B2-B4. R: reference.

initial OFAT experiments. However, the result was not confirmed by these experiments, so experiment A1.10 is probably an incorrect measurement. However, this should not be a major issue, as it was corrected in the second BO round. In the third BO round, even the lowest measured values exceed the productivity-cost ratios of the previous rounds. The highest value reached was 31.9 mmol L^{-1} h^{-1} €$^{-1}$ (Experiment B3.1). For the subsequent experiments, the BO algorithm proposed similar values for the parameters, which indicates that reaction system's region of optimality was narrowed down, and the algorithm entered the exploitation phase. Three experiments were performed with only slight variations in MVK concentrations while keeping the concentrations of the remaining components constant, which led to minor differences in productivity and costs. In the context of BO, these slightly different experiments provide richer information on the shape of the optimization objective around the optimum as compared to one triplicate experiment,[45] however, they have a similar significance in terms of validation. The overall highest productivity-cost ratio of 38.6 mmol L^{-1} h^{-1} €$^{-1}$ was reached using 200 mM phosphate and pyruvate, 0.4 U mL^{-1} POX, 1 U mL^{-1} ACK and 135.8 mg mL^{-1} MVK.

The fourth BO round was manually complemented by an experiment (B4.4) with an increased ADP concentration of 5.5 mM instead of 1 mM. This experiment aimed to assess whether ADP has a higher impact on the optimization objective than previously expected. Here, a slightly higher productivity-cost ratio of 39.8 mmol L^{-1} h^{-1} €$^{-1}$ was reached. The respective values for productivity and costs fall within expected ranges as compared to the prior experiments. This validates the anticipated low impact of ADP on productivity, cost, and the productivity-cost ratio.

Using an overall amount of 52 experiments, we successfully optimized the MVAP-producing and ATP-regenerating enzymatic system, substantially enhancing its productivity-cost ratio using single experiments. This optimization led to a 2fold increase of the productivity-cost ratio as compared to the reference, while maintaining consistent productivity levels. Furthermore, it is to be noticed that the concentration of phosphate and hence, pyruvate is in the upper concentration range. Even higher productivity-cost ratios may be achievable by adjusting the bounds of the parameter space. Allowing higher concentrations and considering phosphate and pyruvate concentrations independently from each other may lead to further improvements of the reported KPIs. It should also be noted that in this study, the cost of POX is approximately four- orders of magnitude higher than of ACK and MVK, as POX was commercially purchased. Hence, its impact on the productivity-cost ratio is more significant. In-house enzyme production or a commercial purchase of all enzymes would lower its influence. However, the data obtained from the experiments can be easily used as a basis to optimize the studied system for other objectives. As demonstrated by the change of the optimization objective BO is a highly versatile approach that can incorporate and utilize information from previous studies. We expect only a few rounds of BO with relatively low experimental effort to be required for optimizing, for example, STY.[34] In the following, the acquired data is further analyzed in terms of the algorithm's behavior, and the usage of single experiments is discussed and justified in more detail.

2.4. Data Analysis

Throughout the BO rounds B1-B4, we observed a narrowing down of the range of proposed experiments, first guided by the productivity and then by the productivity-cost ratio (Figure 4). Notably, the second BO round saw an expansion in the ranges of phosphate and ACK due to a shift in the optimization objective while POX concentration range was significantly reduced, reflecting its disproportionate impact on cost. In the concluding BO round, only the MVK concentration was adjusted, with other variables held constant, which indicates that the algorithm converges to the optimum.

The BO algorithm transitioned from a wider exploratory scope in its first and second rounds to a more precise exploitation of the optimal parameter region in its third and fourth round. This strategic shift is highlighted by the reduced variation in design parameters, ultimately narrowing down to primarily adjusting MVK concentration. This change signals the approach toward refining the most efficient reaction conditions.

Figure 5 offers further insight into how the BO algorithm investigates the parameter space, by example of BO rounds 1 and 2. Assessing the cross-sections of the parameter space in BO round 1 (Figure 5, top), it is evident that the GPR model in this round was still rather uninformed, which is reflected in the wide distribution of sampling locations across the parameter space. Areas with high concentrations of POX and low levels of phosphate and MVK were avoided, based on low performance during the exploratory rounds A1-A3. Notably, the best observation up to this point was made with experiment A1.10. Thus, BO proposes multiple similar experiments (Experiment B1.1, B1.4, B1.6, B1.8) near that point of maximum EI, aiming to improve upon experiment A1.10. In addition, explorative experiments (Experiment B1.2, B1.3, B1.5, B1.7) were proposed at points that exhibit higher GPR model uncertainty (Figure S5), since regions of uncertainty also hold the potential to improve upon the best-measured value.

As shown in Table 5 and Figure 3, the experiments proposed to exploit the region around experiment A1.10 performed substantially worse than expected, leading to a recalibration of the GPR and EI landscape in BO round 2 (Figure 5, bottom). Besides the change of the optimization objective here, the area previously considered promising due to the performance of experiment A1.10 now exhibits substantially lower EI. This change arises because, within the context of the GPR model, the additional experiments have reclassified experiment A1.10 as an outlier. Moreover, the explorative experiments proposed in BO round 1 revealed a new region of interest that is., higher phosphate concentrations and moderate POX levels, into which the BO algorithm eventually converges (Figures S3–S22). Notably, the decrease of overall EI from the BO round 1 to 2 underscores a reduction in uncertainty as the GPR model becomes increasingly informed by accumulating additional data points.

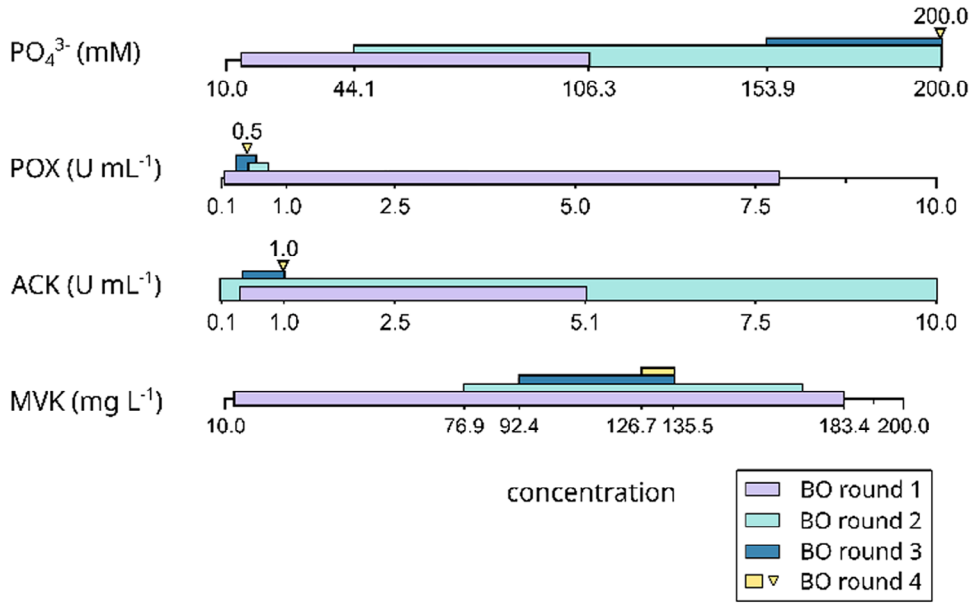

Figure 4. Concentration ranges in which the experiments were proposed during the BO rounds.

Table 6. Outlying experiments with their initial and repeated results.

Experiment	Productivity [mmol L^{-1} h^{-1}]	Costs [€]	Pr/€ [mmol L^{-1} h^{-1} €$^{-1}$]
Previous A1.10	25.1	0.97	25.8
Repeated A1.10	20.6	0.97	21.2
Previous A3.3	77.2	7.62	10.1
Repeated A3.3	44.3	7.62	5.8

Generally, no replicated experiments were conducted as part of this study. However, to validate the inherent outlier classification performed by the GPR model, two experiments were repeated, which were conspicuous due to their high productivity and productivity-cost ratios (Table 6). Aside from experiment A1.10, experiment A3.3 exhibited higher productivity than similar sampling locations with high amounts of phosphate, ACK, and POX (e.g., Experiments A3.4-A3.6). When experiment A3.3 was repeated, it became apparent that it yielded in very similar results to experiments A3.4-A3.6 and therefore the previous experiment (A3.3) was incorrect. At the same time, experiments A3.4-A3.6 were confirmed. Even though no replicates were performed, a validation of the results is therefore given.

The repeated experiments exhibited lower productivity and productivity-cost ratios, confirming that these experiments were outliers. However, the iterative optimization was performed without explicitly identifying or removing such outliers. Notably, this did not impair the optimization process, because high KPIs could not be reproduced and proposals deviated from it, and hence, we have demonstrated that single experiments are sufficient when using BO in the presented case. Avoiding replicates considerably reduces the number of required experiments. The final optimal conditions were verified by performing almost identical experiments with similar concentrations, resulting in similar objective values (Figure 4).

While the iterative optimization using the GPR model with EI showed convergence in the fourth round of BO, and despite mutual validation of the experimental results in the optimal region of the parameter space, it is crucial to verify whether we have indeed identified the optimal process conditions for the studied enzyme cascade. As discussed in the section on isotropic and anisotropic kernel functions in GPR modeling, the GPR model employed for BO of the enzyme cascade used an isotropic kernel function, which may limit the GPR model's ability to capture nuanced differences in the influences of the design parameters. To thoroughly evaluate this approach and the identified optimal reaction conditions, another GPR model employing an anisotropic kernel function was constructed, utilizing the complete final dataset. For an in-depth description of the anisotropic GPR model, refer to the respective section in the Supporting Information. The anisotropic GPR model is used to make a robust assessment regarding the location of the optimum. This is achieved by determining the probability density of the optimal reaction conditions, as depicted in Figure 6. The probability density is obtained by optimizing 10000 functions sampled from the anisotropic GPR model. This procedure is further explained in the section on sampling from GPR models. For further information on GPR models, refer to the section on GPR models and ref. [51].

The resulting analysis allows to identify regions of the parameter space which are most probable to include the optimal experimental conditions under uncertainty. The varying shades depicted in Figure 6 each signify 20% increments in cumulative probability mass. Consequently, we can assess with a 20% probability that the system's optimum lies within the dark blue region and with an 80% probability that the optimum lies within the light blue contours, respectively. Notably, even with the enhanced capacity of the anisotropic GPR model to capture the influence of each parameter, the region with the highest probability of containing the optimum aligns with our

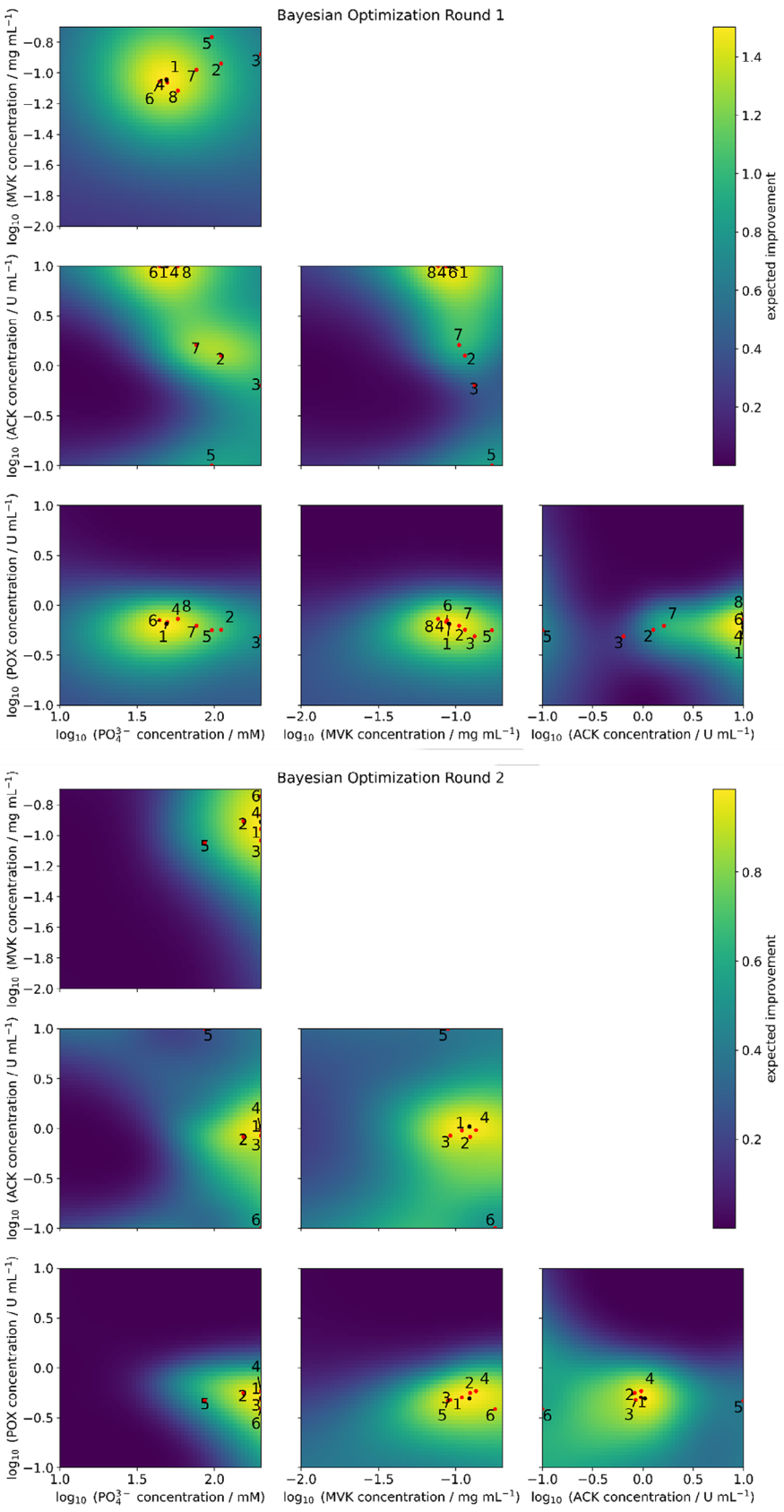

Figure 5. Results of BO rounds 1 (top) and 2 (bottom) with experimental plans. The subplots display two-dimensional cross-sections of the parameter space, intersecting in the point of maximum EI, which is different after each round, represented by black dots. The color intensity of the heat map encodes the EI values for potential experimental conditions, using the "viridis" color map.[69] Red dots indicate the experiments proposed for BO rounds 2 and 3, respectively numbered according to the proposal order as discussed in the section on batch-sequential expected improvement.

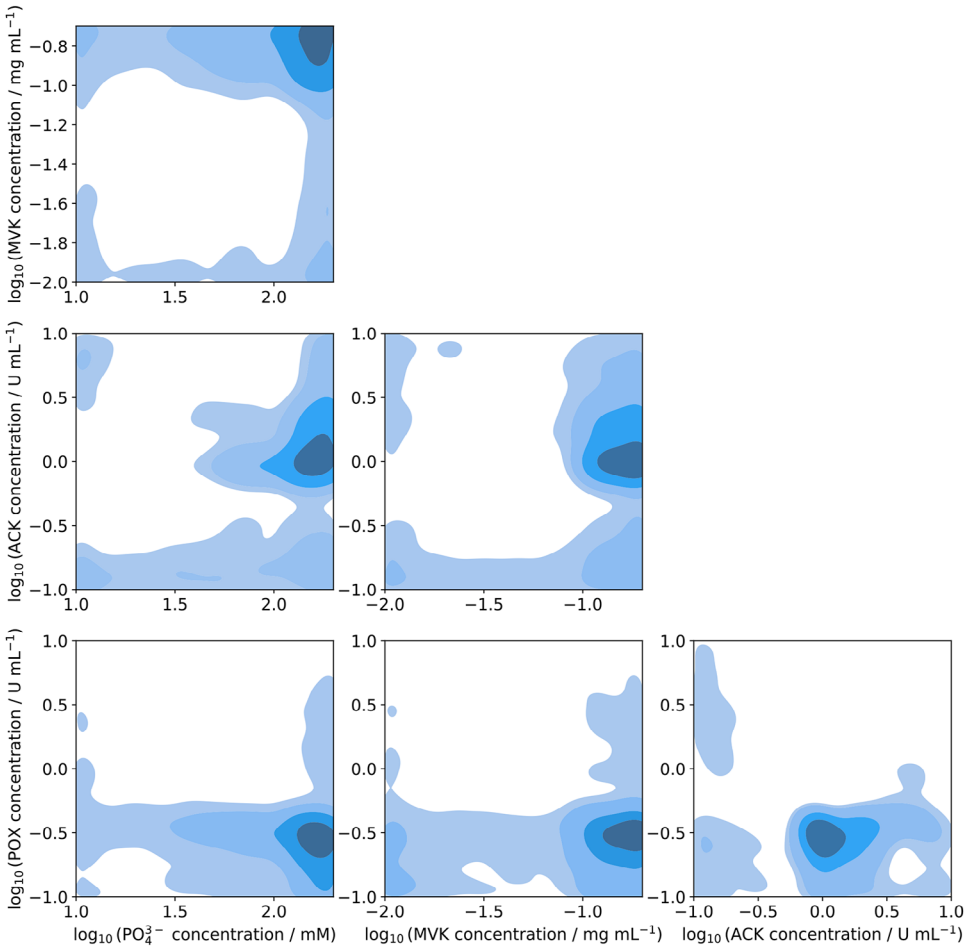

Figure 6. Probability density of the optimal reaction conditions. Contours map cumulative probability mass increments of 20%, The probability density is derived from 10000 functions sampled from an anisotropic GPR model trained on the final dataset build with the Bayesian modelling framework, PyMC.[59] Functions of the GPR model are approximated with random Fourier features,[65] using the pyrff Python library.[66]

previous findings. However, unlike the isotropic GPR model, the anisotropic model includes low-concentration regions of ACK, MVK, and phosphate within the 80% probability area. This is a notable deviation from the isotropic model, which, after the second-round of BO, excluded these low-concentration areas, as evidenced by Figure 5 and Figures S13–S22. The remaining probability assigned to these regions by the anisotropic model is a consequence of the sparse experimental data available there. While the anisotropic model can interpolate densely sampled regions of the parameter space more accurately, extrapolations in less explored regions have a higher uncertainty as compared to the isotropic model. Despite this uncertainty, we are confident that regions with low phosphate concentrations are suboptimal, given that high productivity-cost ratios in this area are expected to correlate with low productivity, primarily due to phosphate limitations. Comparing the cross-sections of the final isotropic (Figure S21) and anisotropic (Figure S24) GPR models demonstrates that, despite the anisotropic model's enhanced ability to independently assess each parameter's impact and its added uncertainty in less sampled areas, the overall approximated landscape of the parameter space remains largely unchanged. Both models offer similar predictions for the productivity-cost ratio. However, the anisotropic model indicates marginally higher ratios across a wider range of phosphate and MVK concentrations and suggests a more confined optimal range for ACK. This underscores the effectiveness of the initial isotropic kernel function assumption for the BO.

3. Conclusions and Outlook

Utilizing BO, an enzymatic system for MVAP production with included ATP regeneration by POX and ACK was optimized for productivity and costs using single experiments. As surrogate model, GPR and as acquisition function, EI was used, though other methods can be chosen. The impacts of parameters on the KPIs were initially determined by an OFAT approach to explore the parameter space. Here, only compound concentrations were considered, but other influencing factors such as temperature or pH can be included as well. The results of the three exploratory rounds indicated that the high-dimensional parameter space could be reduced from seven parameters to four in the following rounds. Based on the combined data of the first three

rounds, only four additional rounds that were designed using BO were necessary to identify the best productivity-cost ratio, which results in 52 experiments in total. Our study demonstrated that single experiments are sufficient for this task, efficiently exploring the parameter space with a focus on regions near high objective values. This way previously measured results are intrinsically validated, and outlying results are compensated, while saving experimental resources. A liquid handling robot could be fully integrated with the BO algorithm to further reduce the work effort. A flexible switch of the optimization objective was demonstrated during the optimization, and with the acquired data set, a rapid optimization for other targets will be possible. Furthermore, a multi-objective optimization also known as Pareto optimization, as it is often needed in enzyme cascades, is feasible in the BO context,[23] for example, by replacing EI by expected hypervolume improvement.[52] Hence, BO is an optimization approach that is applicable to a variety of (biological) systems, which have to be improved in a time and cost-efficient manner.

4. Experimental Section

4.1. Material

Chemicals were purchased from Acros Organics (ThermoFisher Scientific, Waltham, MA, USA), AppliChem (AppliChem GmbH, Darmstadt, Germany), Merck (Merck KGaA, Darmstadt, Germany), Roth (Carl Roth, Karlsruhe, Germany), Santa Cruz Biotechnology (Santa Cruz Biotechnology, Inc., Dallas, TX, USA), TCI (TCI Deutschland GmbH, Eschborn, Germany), ThermoFisher (ThermoFisher Scientific, Waltham, MA, USA), and VWR (VWR international GmbH, Darmstadt, Germany).

4.2. Enzyme Production

The GeneArt Strings DNA Fragments (ThermoFisher Scientific, Waltham, MA, USA) of ACK homologues were purchased and cloned by Gibson Assembly to the PCR amplified pET28b.[53] Primers and gene sequences are listed in Table S1. Correct implementation was confirmed by Sanger Sequencing. Plasmid of MVK was kindly provided by Frank Schulz and both, ACK and MVK were expressed and purified as explained in ref. [35]. POX from *Aerococcus viridans* was purchased from Merck (Merck KgaA, Darmstadt, Germany).

4.3. Enzyme Assays

Enzyme assays were performed with purified enzymes in 1.5 mL Eppendorf tubes, filled up with activity buffer (100 mM Tris-HCl, 150 mM NaCl, 10% glycerol, 20 mM $MgCl_2$, pH 7.5) to a final reaction volume of 0.35 mL. All assays contained additionally 0.1 mM FAD, 0.1 mM ThPP, 20 U mL^{-1} catalase, 20 mM $MgCl_2$, 3 mM Na_3VO_4, 0.043 mM $NADP^+$, 0.43 mM CoA, 170 mM glucose, and 200 mM NaOAc. The latter five components were added because they are crucial for a larger FPP-producing cascade and no MVA-activity was detected without (data not shown).[39] The reaction was incubated for 24 h at 30 °C in a multirotator with 30 rpm to allow for a sufficient oxygen supply. Samples were taken regularly, and enzymes were inactivated at 95 °C for 5 min.

4.4. Analytics

To fit in the linear range of the calibration curve, samples were centrifuged and diluted with water prior to injection. The analytes were measured using a LC-MS (1260 Infinity II LC system combined with 6120 Quadrupole MS (Agilent, Santa Clara, CA, USA)) using a SeQuant ZIC-pHILIC 5 µm polymer 200 Å, 150 × 2.1 mm column (Merck KgaA, Darmstadt, Germany), heated to 40 °C and samples from the fourth BO round were measured using a Poroshell 120 HILIC-Z 2.1 mm × 150 mm, 2.7 µm (Agilent, Santa Clara, CA, USA) heated to 35 °C. The flow rate was set to 0.2 mL min^{-1} and the injection volume was 3 µL. The following gradient of mobile phase A (90% 10 mM NH_4Ac, pH 9.2, 10% acetonitrile) and mobile phase B (90% acetonitrile, 10% 10 mM NH_4Ac, pH 9.2) was used for separation: 0 min: 0% A; 1 min: 0% A; 30 min: 75% A; 34 min: 100% A; 39 min: 100% A, 49 min: 0% A, 64 min 0% A. Negative mode was used for the MS measurements and the parameters for electron spray ionization (ESI) were set to the following: drying gas temperature: 350 °C, nebulizer pressure: 35 psig, drying gas flow: 12 L min^{-1}, capillary voltage: 3500 V. Analytes were detected in the selected ion mode (SIM) with m/z of 147.0 and 147.1 during the first 15 min to detect MVA and 226.9, 227, 227.1, and 455 for monomeric and dimeric MVAP from 15 min to 33 min. Specific activities and productivities were determined from substrate and product concentrations, respectively as initial rates in the linear range.

4.5. Software

In this study, all analyses and visualizations were conducted using Python 3.11. The initial processing of experimental data and the formulation of sampling locations were handled by our in-house software package Planalyze, which is available upon request. Planalyze integrates several Python libraries, including scikit-learn (v1.1.3),[54] NumPy (v1.23.4),[55] SciPy (v1.9.3),[56] pandas (v1.5.1),[57] and xarray (v2022.11.0).[58] For the construction of the anisotropic GPR model, we utilized PyMC (v5.10.3).[59] The visualization of our data and results was facilitated by Matplotlib (v3.6.2)[60] and seaborn (v0.12.1),[61] with ArViz (v0.17.0)[62] providing additional support for statistical graphics.

4.6. Gaussian Process Regression Modeling

BO of complex biochemical processes, such as enzyme cascades with multiple design parameters, requires regression models capable of capturing nonlinear relationships between design parameters and performance indicators. These models must also handle noisy measurements of the observed ground-truth system behavior. In this study, we use GPR models for that task. GPR models, which employ Gaussian Processes (GPs) for regression purposes, are non-parametric, that is, they do not assume a specific parametric form to explain the functional dependency of KPIs on design parameters. GPs are distributions over infinitely many functions that can potentially explain the observed data. The fitting of a GP involves not only the match of the model to the data but also the smoothness and variability of the approximating functions, all while accounting for prior information on the underlying system. This way, GPs can infer the likelihood of each function that potentially explains the data. Moreover, they can inherently quantify the uncertainty of their own predictions. These two features are instrumental for guiding optimal experimental design.

A GP is defined by a mean function and a covariance function. The mean function represents the average output across the parameter space, serving as a baseline prediction. The covariance

function, defined in part by its length scale, determines the similarity between different points in the parameter space. It governs how the GP generalizes from observed data to unexplored areas of the parameter space, with the length scale shaping both the correlation and the rate of change across the parameter space.

In this study, the GP was parametrized with a mean function of zero, which is a common choice in many applications.[22,25,63] By default, GPs assume that input data can span the entire spectrum of real numbers. However, this study's design parameters – substrate and enzyme concentrations – are strictly positive. To accommodate this constraint, these domains are mapped by log-transforming all input data. This approach offers the added benefit of linearizing the relationship between design parameters and observations, aiding the GPR model in more effectively interpreting and predicting the system's behavior across a broad range of parameter values.

For the covariance function, the sum of a Matérn kernel and a white noise kernel was selected. This choice enables the model to represent 1) smooth variations of the underlying biological system (Matérn kernel) and 2) uncorrelated noise (white noise kernel), which is inherent to all measurements in biocatalysis. We assume that the objective values, that is, productivity or productivity-cost ratio, vary smoothly in response to changes in the design parameters. Hence, we set the prior of the length scale to half the extent of the logarithmically transformed parameter ranges.

4.7. Isotropic and Anisotropic Kernel Functions in Gaussian Process Modeling

The initial dataset utilized for fitting the GPR model predominantly consists of OFAT experiments, where each data point uniquely varies in just a single parameter. Consequently, the resulting sparse and uneven distribution of data points presents a considerable risk of overfitting the GPR model. To mitigate this issue, an isotropic kernel function was selected for the GPR model during BO. Isotropic kernel functions are characterized by uniform length scales across all input dimensions. This uniformity assumes a consistent rate of change in the GPR model's response, regardless of the direction in the parameter space which offers multiple advantages. Notably, it reduces the risk of overfitting and facilitates a faster identification of the region of optimality. However, while the uniform learning of isotropic kernel functions throughout the parameter space is beneficial in this context, it can also have limitations. Specifically, GPR models using isotropic kernel functions may struggle to adequately capture complex interactions and varying impacts of different parameters on the studied performance indicators, potentially leading to suboptimal experiment proposals. In contrast, anisotropic kernel functions, which feature distinct length scales for each dimension, provide a more adaptable approach. This additional flexibility of adjusting the length scales to each parameter of the system enables the model to more accurately represent regions of the parameter space that exhibit particularly heterogeneous behavior. To evaluate this potential shortcoming of isotropic kernel functions and validate our initial assumption, we constructed a second GPR model with an anisotropic kernel function based on the final dataset of BO. This model, tailored to acknowledge varying scales of influence across all parameters, was used for generating the probability density plot shown in Figure 6. A detailed description of the anisotropic GPR model can be found in the Supporting Information.

4.8. Batch-sequential Expected Improvement

To propose sampling locations, we utilized EI as acquisition function. It predicts the expected amount of improvement at any given point in the parameter space, relative to the current best observation. These predictions are based on both the mean and variance of the underlying GPR model. EI balances between exploring less sampled regions and exploiting known promising areas. It predicts one optimal experiment at a time. Given the practical time and cost-related constraints in this study, we applied a so-called batch-sequential approach for proposing up to 8 experiments that can be executed simultaneously in each round of BO. In this approach, EI is repeatedly applied to propose optimal experiments, while temporarily updating the GPR model with its own predictions of each proposed experiment until the number of desired experiments is reached. The temporary data are subsequently removed from the database and replaced by the observed measurements.

4.9. Sampling From Gaussian Process Regression Models

GPR models can be conceptualized as probability distributions over functions that fit a given dataset. By employing such a GPR model, the location of the system's optimum under uncertainty can be determined by calculating the probability density of the optimal reaction conditions, as depicted in Figure 6.

In our study, this is achieved by sampling a sufficiently large number of functions from the anisotropic GPR model and subsequently determining the location of the maximum for each sampled function. By examining the distribution of these maxima, we can assess the probability for each region within the parameter space to contain the optimum of the underlying system. However, there are no known methods to directly sample exact functions from a GPR model.[23] A commonly applied alternative to this is to sample analytic approximations[23,25] of these functions which can be efficiently evaluated and optimized. In our study, we utilize random Fourier features approximations (RFF),[64,65] to approximate functions sampled from the anisotropic GPR model. These RFF approximations are calculated using the pyrff Python library.[66] For a visual comparison, a side-by-side illustration of sample functions drawn from the anisotropic GPR model and their RFF approximations is provided in the Supporting Information (Figure S23).

Supporting Information

The authors have cited additional references within the Supporting Information.[67,68]

Acknowledgments

Regine Siedentop received funding by the Deutsche Forschungsgemeinschaft (DFG) under the priority programme SPP 2240 "eBiotech" (Bioelectrochemical and engineering fundamentals to establish electro-biotechnology for biosynthesis-Power to value-added products) (grant agreement No 445751305). Additionally, Maximilian Siska performed this work as part of the Helmholtz School for Data Science in Life, Earth and Energy (HDS-LEE) and received funding from the Helmholtz Association of German Research Centres. The authors would like to acknowledge the support with analytics by Sascha Nehring and Don Marvin Voss. We would also like to express gratitude to Michael Osthege for his valuable insights and input into the modeling aspects of this research. Special thanks are extended to Frank Schulz for

providing the plasmid of MVK and to Charlotte Knoop for her preceding work.

Open access funding enabled and organized by Projekt DEAL.

Conflict of Interests

The authors declare no conflict of interest.

Data Availability Statement

The data that support the findings of this study are available from the corresponding author upon reasonable request.

Keywords: ATP regeneration · Bayesian optimization · Biocatalysis · Gaussian process regression · Machine learning

[1] E. Erdem, J. M. Woodley, *Chem. Catalysis* **2022**, *2*, 2499–2505.
[2] M. Teshima, et al., *Curr. Opin. Biotechnol.* **2023**, *79*, 102868.
[3] R. J. Young, et al., *JACS. Au.* **2022**, *2*, 2400–2416.
[4] F. H. Arnold, *Angew Chem. Int. Ed. Engl.* **2018**, *57*, 4143–4148.
[5] K. Rosenthal, et al., *Angew Chem. Int. Ed. Engl.* **2022**, *61*, e202208358.
[6] A. I. Benítez-Mateos, et al., *Nat. Chem.* **2022**, *14*, 489–499.
[7] *Enzyme Cascade Design and Modelling* (Eds: S. Kara, F. Rudroff), Springer, Cham **2021**.
[8] D. Ribeaucourt, et al., *ACS Catal.* **2022**, *12*, 1111–1116.
[9] K. Petroll, et al., *Biotechnol. Adv.* **2019**, *37*, 91–108.
[10] J. N. Andexer, M. Richter, *ChemBioChem* **2015**, *16*, 380–386.
[11] K. Murata, et al., *Agric. Biol. Chem.* **1988**, *52*, 1471–1477.
[12] T. Noguchi, T. Shiba, *Biosci. Biotechnol. Biochem.* **1998**, *62*, 1594–1596.
[13] Y.-S. Shih, G. M. Whitesides, *J. Org. Chem.* **1977**, *42*, 4165–4166.
[14] B. L. Hirschbein, et al., *J. Org. Chem.* **1982**, *47*, 3765–3766.
[15] D.-M. Kim, J. R. Swartz, *Biotechnol. Bioeng.* **1999**, *66*, 180–188.
[16] J. A. McIntosh, et al., *ACS Cent. Sci.* **2021**, *7*, 1980–1985.
[17] Z. Du, et al., *iScience* **2021**, *24*, 102236.
[18] R. Siedentop, et al., *ChemElectroChem* **2023**, *10*, e202300332.
[19] S. Ruccolo, et al., *J. Am. Chem. Soc.* **2022**, *144*, 22582–22588.
[20] R. Siedentop, et al., *Catalysts* **2021**, *11*, 1183.
[21] L. Paschalidis, et al., *Biochem. Eng. J.* **2022**, *181*, 108384.
[22] E. Bradford, et al., *Comput. Chem. Eng.* **2018**, *118*, 143–158.
[23] E. Bradford, et al., *J. Glob. Optim.* **2018**, *71*, 407–438.
[24] L. Freier, E. von Lieres, *Biotechnol. J.* **2017**, *12*, 1600613.
[25] N. von den Eichen, et al., *Bioprocess Biosyst. Eng.* **2022**, *45*, 1939–1954.
[26] F. Di Fiore, et al., *Arch. Computat. Methods Eng.* **2024**, *31*, 2985–3013.
[27] S. Greenhill, et al., *IEEE Access* **2020**, *8*, 13937–13948.
[28] P. I. Frazier, *arXiv.org*, **2018**, https://doi.org/10.48550/arXiv.1807.02811.
[29] G. De Ath, et al., *ACM Trans. Evol. Learn. Optim.* **2021**, *1*, 1–22.
[30] B. Shahriari, et al., *Proc. IEEE Inst. Electr. Electron. Eng.* **2016**, *104*, 148–175.
[31] L. Freier, et al., *Eng. Life Sci.* **2016**, *16*, 538–549.
[32] Y. Saito, et al., *ACS Synth. Biol.* **2018**, *7*, 2014–2022.
[33] B. J. Shields, et al., *Nature* **2021**, *590*, 89–96.
[34] A. Pandi, et al., *Nat. Commun.* **2022**, *13*, 3876.
[35] R. Siedentop, et al., *Catalysts* **2023**, *13*, 468.
[36] R. Tachibana, et al., *ACS Sustain Chem. Eng.* **2023**, *11*, 12336–12344.
[37] F. Li, et al., *Nat. Catal.* **2022**, *5*, 662–672.
[38] M. Mukherjee, et al., *Metab. Eng.* **2022**, *74*, 139–149.
[39] M. Dirkmann, et al., *ChemBioChem* **2018**, *19*, 2146–2151.
[40] S. Sundaram, et al., *Angew. Chem. Int. Ed.* **2021**, *60*, 16420–16425.
[41] T. P. Korman, et al., *Nat. Commun.* **2017**, *8*, 15526.
[42] R. Siedentop, et al., *Chem. Ing. Tech.* **2023**, *95*, 543–548.
[43] G. Suryatin Alim, et al., *Adv. Biochem. Eng./Biotechnol.* **2023**, 29–49, https://doi.org/10.1007/10_2023_222.
[44] N. Huber, et al., *Metab. Eng.* **2024**, *81*, 10–25.
[45] J. Kreyling, et al., *Ecol. Lett.* **2018**, *21*, 1629–1638.
[46] L. M. Helleckes, et al., *Biotechnol. Bioeng.* **2023**, *120*, 139–153.
[47] R. Siedentop, et al., *Catalysts* **2023**, *13*, https://doi.org/10.3390/catal13030468.
[48] J. Lu, J. Zhang, *RSC Adv.* **2019**, https://doi.org/10.1039/C9RA04765D.
[49] E. Radley, et al., *Angew. Chem., Int. Ed.* **2023**, *62*, e202309305.
[50] Ó. Ögmundarson, et al., *Trends Biotechnol.* **2020**, *38*, 1203–121.
[51] C. E. Rasmussen, in *Lecture Notes in Computer Science*, Vol. *3176*, Springer, Berlin **2004**, pp. 63–71.
[52] L. Freier, E. von Lieres, *Biotechnol. J.* **2018**, *13*, 1700257.
[53] D. G. Gibson, et al., *Nat. Methods* **2009**, *6*, 343–345.
[54] F. Pedregosa, et al., *J. Mach. Learn. Res.* **2011**.
[55] C. R. Harris, et al., *Nature* **2020**, *585*, 357–362.
[56] P. Virtanen, et al., *Nat. Methods* **2020**, *17*, 261–272.
[57] W. McKinney, *Proceedings of the 9th Python in Science Conference*, **2010**, https://doi.org/10.25080/Majora-92bf1922-00a.
[58] S. Hoyer, J. Hamman, *J. Open. Res. Softw.* **2017**, *5*, https://doi.org/10.5334/jors.148.
[59] O. Abril-Pla, et al., *Peer J. Comput. Sci.* **2023**, https://doi.org/10.7717/peerj-cs.1516.
[60] J. D. Hunter, *Comput. Sci. Eng.* **2007**, *9*, 90–95.
[61] M. Waskom, *J. Open Source Softw.* **2021**, *6*, 3021.
[62] R. Kumar, et al., *J. Open Source Softw.* **2019**, *4*, 1143.
[63] C. E. Rasmussen, C. K. I. Williams, *Gaussian Processes for Machine Learning*, The MIT Press, **2005**.
[64] A. Rahimi, B. Recht, *Advances in Neural Information Processing Systems*, Vol. *20*, NIPS Curran Associates, Red Hook, NY, USA, **2007**.
[65] J. M. Hernández-Lobato, et al., in *NIPS'14: Proceedings of the 27th International Conference on Neural Information Processing Systems*, Vol. 1, MIT Press, Cambridge, MA, USA, **2014**, pp. 918–926.
[66] M. Osthege, K. Felton, *Zenodo* **2022**, https://doi.org/10.5281/ZENODO.6583770.
[67] P. Tufvesson, et al., *Org. Process Res. Dev.* **2011**, *15*, 266–274.
[68] M. D. Hoffman, A. Gelman, *J. Mach Learn Res.* **2014**, https://doi.org/10.5555/2627435.2638586
[69] Colormap reference — Matplotlib 3.8.2 documentation, https://matplotlib.org/3.8.2/gallery/color/colormap_reference.html.

Manuscript received: April 30, 2024
Revised manuscript received: June 21, 2024
Accepted manuscript online: September 15, 2024
Version of record online: September 28, 2024
[Correction added on 1 October 2024, after first online publication: The article's title was updated in this version.]